Enhancement of Spin Current Polarization in 2D Ferromagnetic/Insulator/Heavy Fermion Material Tunnel Junction Induced by Rashba Spin–Orbit Coupling

A. Poszwa*

Faculty of Mathematics and Computer Science, University of Warmia and Mazury in Olsztyn, Słoneczna 54, 10-710 Olsztyn, Poland

Received: 22.06.2022 & Accepted: 10.11.2022

Doi: 10.12693/APhysPolA.143.55 *e-mail: poszwa@matman.uwm.edu.pl

A theoretical investigation of the spin- and charge transport properties of the ferromagnetic metal/insulator/heavy fermion Rashba metal tunnel junction is presented. The electron dynamics in the entire system are described within a single-particle effective Hamiltonian. The dependence of the spin current polarization and the low-bias spin-resolved conductance spectra on the macroscopic parameters of the system are studied. We consider an infinite two-dimensional system with periodic boundary conditions imposed along the transverse direction of the junction. We observed that strong spin current polarization amplification and spin current filtering are induced by Rashba spin–orbit coupling in the presence of a large effective masses difference between ferromagnetic metal and heavy fermion Rashba material. The spin-dependent scattering problem is solved analytically within the effective mass approximation in combination with the spin density matrix formalism.

topics: spin current, tunnel junction, conductance

1. Introduction

Electronic transport in low-dimensional systems with Rashba-type spin–orbit interaction (RSO) has attracted a lot of attention due to the promising properties of spin states whose dynamics may be controlled effectively by an externally applied electric field [1–5]. The classic example is the Datta–Das proposal of the ballistic spin field effect transistor, where the spin precession length is controlled by varying RSO strength in a semiconductor region, driving the charge current between two ferromagnetic contacts [6]. One of the central themes of spintronics research is thus the study of the interplay between spin- and charge transport in various heterostructures [7–12]. At this stage, the large tunneling magnetoresistance observed in magnetic tunnel junctions (MTJs) garnered much attention due to possible applications in nanotechnology, particularly in the fabrication of random access memories and next-generation magnetic field sensors [13]. The fundamental property of an MTJ is that the tunneling current depends on the relative orientation of the magnetizations of the two ferromagnetic contacts. This phenomenon is referred to as tunneling magnetoresistance (TMR). TMR is related to spin-dependent tunneling (SDT). The SDT reflects an imbalance in the electric current carried by up- and down-spin electrons tunneling through the potential barrier, separating ferromagnetic electrodes. The origin of SDT can be explained by the fact that the tunneling probability depends on the Fermi wave vector. As is well known, in ferromagnetic metals electronic bands are exchange-split, which gives different Fermi wave vectors for up- and down-spin electrons. As a consequence, a tunneling probability becomes spin-dependent. The SDT effect has been studied extensively in various contexts. The tunneling anisotropic magnetoresistance effect in ferroelectric tunnel junctions with ferromagnetic and normal metal electrodes separated by a ferroelectric barrier of finite thickness has been studied, including both Rashba and Dresselhaus spin–orbit coupling [14]. The possibility to control the resistance through ferroelectric polarization of the barrier and through magnetization configuration of the electrodes has been demonstrated in a frame of the model of multiferroic tunnel junction, which explicitly includes the spin-dependent screening potential [15]. The charge and spin transport through a junction composed of an ordinary two-dimensional metal and a non-centrosymmetric two-dimensional semiconductor with RSO have been studied using the free electron approximation and scattering method [16]. A complete description of tunneling transport and interface properties of Schottky diodes in the non-linear rectifying regime has been recently performed experimentally [17]. Direct and phonon-assisted interband tunneling transport have been studied theoretically

based on the self-consistent solution of Poisson's and Schrödinger's equations within effective mass approximation [18]. The double junction systems of ferromagnet/superconductor/ferromagnet have been studied within the one-band approximation [19, 20]. Many theoretical investigations have shown that both charge and spin transport in hybrid structures between the Rashba system and various materials such as metals [21–23], ferromagnets [24–27], and superconductors [28] are affected by the strength of RSO.

Heavy fermion materials (HFMs) play an important role in current scientific research, acting as prototypical materials for non-Fermi liquid behavior, unconventional superconductivity, and quantum criticality [29]. The actual interaction between conduction electrons and localized f-magnetic moments in HFM is still not completely understood and is a topic of ongoing experimental and theoretical investigations. HFMs belong to the group of strongly correlated electron systems. In HFM, the non-perturbative growth of the interaction leads to quasi-electrons with masses up to thousands of times the bare electron mass, i.e., the electrons are dramatically slowed by the interactions. Heavy fermion behavior has been found in a wide variety of states, including superconducting, metallic, insulating, and magnetic states. Typical examples are $CeCu_6$, $CeAl_3$, $CeCu_2Si_2$, $YbAl_3$, UBe_{13}, and UPt_3. At high temperatures, HFM exhibit a large saturated resistivity, induced by incoherent spin-flip scattering of the conduction electrons on the local f-moments. This scattering becomes increasingly elastic as the temperature is lowered. In the case of HFM, the development of coherence manifests itself by a rapid reduction in resistivity. The localized magnetic moments become screened by the spins of the conduction sea and ultimately form a spinless scattering center at low temperatures. This is the regime of asymptotic freedom [30]. Heavy fermion materials are strongly correlated systems, and a comprehensive description of the electron dynamics in such materials needs to use some Kondo lattice-type Hamiltonian [31]. However, in the first approximation, we employ a single-particle Hamiltonian as in the case of semiconductors or metals, but with a larger effective mass. One should note that above the characteristic coherence temperature T_{coh}, HFMs behave like normal metals. Compared to a normal metal, however, HFMs at higher temperatures have a high scattering rate due to the large density of local magnetic moments (at least one f-electron per unit cell), which cause incoherent Kondo scattering [32]. Additionally, coherent heavy-electron propagation is readily destroyed by substitutional impurities and the influence of thermal fluctuations of the local spins.

In this paper, we investigate theoretically spin and particle currents through the tunnel junction composed of ferromagnetic metal (FM)/insulator/heavy fermion Rashba metal (HFRM) within the effective mass approximation. In particular, we study the conditions under which the junction acts as the spin current amplifier and the spin current valve. The interference effects between spin-resolved energy eigenstates in every part of the system are neglected, taking into account the electron dynamics in the HFRM material within the effective single-particle treatment. Due to the presence of a magnetization vector, along which the electrons spins are aligned, the FM electrode is the source of well-defined spin-polarized currents. The initial polarization of the currents can be strengthened or suppressed due to the Rashba spin–orbit interaction occurring in the drain electrode, where the effective electron mass is larger compared to the free electron mass. As we will see, some effects are amplified due to this difference. At this point, one should note that the d-electrons in transition metals have a much larger effective mass than the free electron mass, and such materials may also be considered as the source of a large mass difference between two parts of the junction.

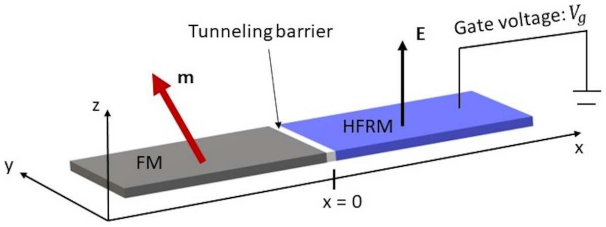

Fig. 1. Schematic of the FM/HFRM tunnel junction. HFRM is applied by the electric field $\boldsymbol{E}$ perpendicular to the plane of the system. The electric field is the source of Rashba spin–orbit coupling.

2. Model

The junction is represented by s two-dimensional system, where semi-infinite FM occupies the $x < 0$ region and semi-infinite HFRM occupies the $x > 0$ region, and an insulating layer separating the two regions is situated at $x = 0$. The potential barrier of the insulating interface is taken in the form of the Dirac delta function, which is appropriate for modeling an extremely thin insulating layer. The geometry of the system is shown in Fig. 1.

It is convenient for further analysis to introduce atomic units: $a_0 = \frac{4\pi\varepsilon_0\hbar^2}{m_e e^2}$ as the unit of length, $E_h = \frac{m_e e^4}{(4\pi\varepsilon_0)^2\hbar^2}$ as the unit of energy, and $\alpha_0 = e^2/4\pi\varepsilon_0$ as the unit of Rashba coupling constant [33]. We note that the electron charge used in these definitions is $e = 1.60218 \times 10^{-19}$ C and $\varepsilon_0 = 8.85419 \times 10^{-12}$ F/m. In atomic units, the Hamiltonian of the system reads

$$\hat{H} = \gamma\delta(x) + \begin{cases} \hat{H}_{\mathrm{FM}} & \text{if } x < 0 \\ \hat{H}_{\mathrm{HFRM}} & \text{if } x \geq 0 \end{cases}, \tag{1}$$

where

$$\hat{H}_{\mathrm{FM}} = -\frac{1}{2M_1}(\partial_x^2 + \partial_y^2) + \Delta\, \boldsymbol{m}\cdot\boldsymbol{\sigma},$$
$$\hat{H}_{\mathrm{HFRM}} = -\frac{1}{2M_2}(\partial_x^2 + \partial_y^2) - \mathrm{i}\alpha(\sigma_x\partial_y - \sigma_y\partial_x). \tag{2}$$

Here Δ is the spin-splitting energy in the ferromagnetic material, γ is the effective strength of the potential barrier, and σ's are the Pauli matrices. The unit vector

$$\boldsymbol{m} = \Big[\sin(\Theta)\cos(\phi), \sin(\Theta)\sin(\phi), \cos(\Theta)\Big] \tag{3}$$

indicates the direction of the magnetization of FM, $M_1 \equiv M_{\mathrm{FM}}/m_e$, $M_2 \equiv M_{\mathrm{HFRM}}/m_e$ are effective masses in units of free electron mass m_e, and α is given in units of $\alpha_0 = 1.43996$ eV nm. The energy bands of corresponding parts of the system are given in Fig. 2. The notation used is defined below.

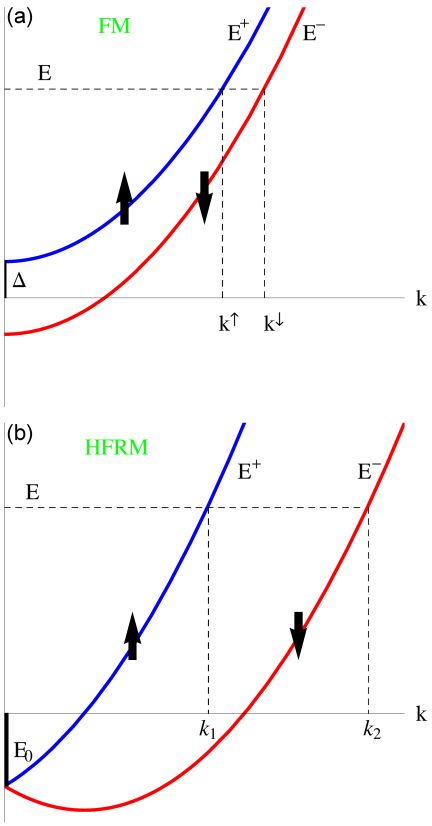

Fig. 2. Energy dispersion along the fixed direction in 2D space of the wavevector $\boldsymbol{k}$ as a function of $k = |\boldsymbol{k}|$ for (a) FM and (b) HFRM materials. Arrows indicate the spin states, given by (4) and (10), respectively. The energy of the incident electron and the Fermi level are measured from the bottom of the minority carriers dispersion in FM. If the FM and HFRM materials are connected, the Fermi level is the same for both parts of the junction. The parameter Δ is the built-in energy splitting between majority and minority carriers spin states in the FM material (exchange energy). For HFRM, the energy shift $E_0 = eV_g$ is controlled by an external gate.

2.1. The FM eigenstates

The Hamiltonian of the ferromagnetic part of the junction has the form of the sum of two terms dependent on the spatial and spin variables, respectively. Thus, the eigenstates of the Hamiltonian $\hat{H}_{\mathrm{FM}}$ can be represented as a product of spatial- and spin-part. The diagonalization of exchange coupling operator $\Delta\,\boldsymbol{m}\cdot\boldsymbol{\sigma}$ gives eigenstates having the form of two-component spinors

$$\chi^{(\uparrow)} = \begin{bmatrix} c \\ s \end{bmatrix}, \quad \chi^{(\downarrow)} = \begin{bmatrix} -s^* \\ c^* \end{bmatrix}, \tag{4}$$

where

$$c = \mathrm{e}^{-\mathrm{i}\phi/2}\cos\left(\frac{\Theta}{2}\right), \quad s = \mathrm{e}^{\mathrm{i}\phi/2}\sin\left(\frac{\Theta}{2}\right). \tag{5}$$

The spinors correspond to the eigenvalues ± 1, respectively. Looking for eigenstates of $\hat{H}_{\mathrm{FM}}$ in the form

$$\mathrm{e}^{\mathrm{i}k_y y}\mathrm{e}^{\mathrm{i}k_x x}\chi^{(\uparrow)}, \quad \mathrm{e}^{\mathrm{i}k_y y}\mathrm{e}^{\mathrm{i}k_x x}\chi^{(\downarrow)}, \tag{6}$$

we obtain corresponding energy dispersion relations

$$E^{\pm}(\boldsymbol{k}) = \frac{k^2}{2M_1} \pm \Delta, \tag{7}$$

where $k = \sqrt{k_x^2 + k_y^2}$. Solving the above equations with respect to k, for $E > \Delta$, one obtains two magnitudes of the wave vector corresponding to minority and majority carriers with the same energy,

$$k^{\uparrow\downarrow}(E) = \sqrt{2M_1\big(E \mp \Delta\big)}. \tag{8}$$

For energies satisfying the condition $-\Delta \le E \le \Delta$, we obtain one solution,

$$k^{\downarrow}(E) = \sqrt{2M_1\big(E + \Delta\big)}. \tag{9}$$

We will consider in this paper only the energy range with two solutions given in (8).

2.2. The HFRM eigenstates

Assuming translational symmetry in both spatial directions, the eigenstates to the spin–orbit operator $\alpha\,(\sigma_x p_y - \sigma_y p_x)$ can be found as the $\boldsymbol{k}$-dependent spinors, known as Rashba spinors, which can be written in the forms

$$\xi^{(1)}(k_x, k_y) = \frac{1}{\sqrt{1+|z|^2}}\begin{bmatrix} 1 \\ -\mathrm{i}z \end{bmatrix},$$
$$\xi^{(2)}(k_x, k_y) = \frac{1}{\sqrt{1+|z|^2}}\begin{bmatrix} 1 \\ \mathrm{i}z \end{bmatrix}, \tag{10}$$

where

$$z = \frac{\alpha}{|\alpha|}\frac{k_x + \mathrm{i}k_y}{k}. \tag{11}$$

We note that when k_x, k_y are real, then $|z| = 1$. However, the wave function of the transmitted electrons may also include an evanescent wave contribution. Evanescent waves correspond to complex components k_x of the Bloch wavevector $\boldsymbol{k}$, corresponding to transmitted electrons. Since $k_x = \sqrt{k^2 - k_y^2}$, where k_y is limited only by the magnitude of the

Fermi vector of incident electrons, the component k_y may exceed the magnitude of the Bloch wavevector of transmitted electrons that leads to complex solutions for k_x. The complex components of the wave vector $\boldsymbol{k}$ lead to the evanescent waves that do not contribute directly to the spin- or charge current for a sufficiently large distance from the scattering region. The complex k_x must be, however, taken into account for the correct calculation of the transmission coefficients satisfying appropriate linear systems (see Appendix A).

Looking for the eigenstates to the Hamiltonian $\hat{H}_{\mathrm{HFRM}}$ in the form

$$\mathrm{e}^{\mathrm{i}k_y y}\mathrm{e}^{\mathrm{i}k_x x}\,\xi^{(1)}(k_x,k_y), \quad \mathrm{e}^{\mathrm{i}k_y y}\mathrm{e}^{\mathrm{i}k_x x}\,\xi^{(2)}(k_x,k_y), \tag{12}$$

we obtain, respectively, two energy dispersion relations

$$E^{\pm}(\boldsymbol{k}) = \frac{k^2}{2M_2} \pm |\alpha|k - E_0, \tag{13}$$

where $E_0 = eV_g$ is energy shift that is defined by an external gate. The magnitudes of the wave vectors corresponding to the branches $\pm$, for fixed energy $E > -E_0$, read

$$k_{1(2)} = \sqrt{2M_2\big(E+E_0\big) + \big(M_2\alpha\big)^2} \mp M_2|\alpha|. \tag{14}$$

For the energy range $-\frac{1}{2}M_2\alpha^2 - E_0 < E < -E_0$, one obtains

$$k_2^{\pm} = \pm\sqrt{2M_2\big(E+E_0\big) + \big(M_2\alpha\big)^2} + M_2|\alpha|. \tag{15}$$

We will consider in further calculations only the case $E > -E_0$. Note that the solutions for semi-infinite contacts are the same as long as we do not impose specific boundary conditions.

2.3. Scattering problem

In the ferromagnetic material, the scattering of incident waves associated with majority-spin and minority-spin electrons may be treated as processes occurring in two independent spin channels. We denote these channels as spin-up ($\uparrow$) if the electron spin is parallel to the vector $\boldsymbol{m}$ and as spin-down ($\downarrow$) if the electron spin is antiparallel to the magnetization vector. For the channel ($\uparrow$), the solution to the Schrödinger equation of the entire system reads

$$\psi^{\uparrow}(y,x) = \mathrm{e}^{\mathrm{i}k_y y}\begin{cases} \mathrm{e}^{\mathrm{i}k_x^{\uparrow}x}\,\chi^{(\uparrow)} + r_p^{\uparrow}\mathrm{e}^{-\mathrm{i}k_x^{\uparrow}x}\,\chi^{(\uparrow)} + r_a^{\uparrow}\mathrm{e}^{-\mathrm{i}k_x^{\downarrow}x}\,\chi^{(\downarrow)}, & x \le 0 \\ t_1^{\uparrow}\mathrm{e}^{\mathrm{i}k_{1x}x}\,\xi^{(1)}(k_{1x},k_y) + t_2^{\uparrow}\mathrm{e}^{\mathrm{i}k_{2x}x}\,\xi^{(2)}(k_{2x},k_y), & x \ge 0. \end{cases} \tag{16}$$

Similarly, for the channel ($\downarrow$), we have

$$\psi^{\downarrow}(y,x) = \mathrm{e}^{\mathrm{i}k_y y}\begin{cases} \mathrm{e}^{\mathrm{i}k_x^{\downarrow}x}\,\chi^{(\downarrow)} + r_p^{\downarrow}\mathrm{e}^{-\mathrm{i}k_x^{\downarrow}x}\,\chi^{(\downarrow)} + r_a^{\downarrow}\mathrm{e}^{-\mathrm{i}k_x^{\uparrow}x}\,\chi^{(\uparrow)}, & x \le 0 \\ t_1^{\downarrow}\,\mathrm{e}^{\mathrm{i}k_{1x}x}\,\xi^{(1)}(k_{1x},k_y) + t_2^{\downarrow}\mathrm{e}^{\mathrm{i}k_{2x}x}\,\xi^{(2)}(k_{2x},k_y), & x \ge 0, \end{cases} \tag{17}$$

where $k_x^{\uparrow\downarrow} = \sqrt{(k^{\uparrow\downarrow})^2 - k_y^2}$, and $k_{ix} = \sqrt{k_i^2 - k_y^2}$, for $i = 1, 2$. For a given Fermi wave vector corresponding to the channel ($\uparrow$) or ($\downarrow$) of the incident wave, we obtain, respectively, the limitation on the k_y component of the Bloch wave vector for transmitted wave, $-k^{\uparrow}(E) \le k_y \le k^{\uparrow}(E)$ or $-k^{\downarrow}(E) \le k_y \le k^{\downarrow}(E)$. By imposing, separately for the spin-up and spin-down channel, following boundary conditions at the interface [34]

$$\psi^{\uparrow\downarrow}(y,0-) = \psi^{\uparrow\downarrow}(y,0+), \tag{18}$$

$$\frac{1}{M_1}\partial_x\psi^{\uparrow\downarrow}(y,x)\Big|_{x=0-} = \left(\frac{1}{M_2} - 2\mathrm{i}\alpha\sigma_y\right)\partial_x\psi^{\uparrow\downarrow}(y,x)\Big|_{x=0+} - 2\gamma\psi^{\uparrow\downarrow}(y,0), \tag{19}$$

we obtain four linear equations for reflection and transmission coefficients $r_p^{\uparrow\downarrow}(E,k_y)$, $r_a^{\uparrow\downarrow}(E,k_y)$, $t_1^{\uparrow\downarrow}(E,k_y)$, $t_2^{\uparrow\downarrow}(E,k_y)$. The systems of equations are given in Appendix A.

3. Spin current and particle current

In the investigation of spin-dependent transport properties, it is convenient to introduce the concept of spin current and particle current densities. The former is defined as the expectation value of the spin current operator, and the latter simply as the expectation value of the velocity operator. The related current density, in this case, is referred to as the particle current or the charge current if the velocity operator is multiplied by the elementary charge. The spin current operator is commonly defined as the product of the velocity operator and the spin operator [35]. According to the general quantum mechanical principle, the x-component of the velocity operator (in a.u.) can be obtained as

$$\hat{v}_x = \mathrm{i}\big[\hat{H}, x\big] = \begin{cases} \frac{p_x}{M_1} & \text{if } x < 0 \\ \frac{p_x}{M_2} - \alpha\sigma_y & \text{if } x \ge 0, \end{cases} \tag{20}$$

where $p_x = -\mathrm{i}\partial_x$. The x-component of the spin current operator takes the form

$$\hat{\boldsymbol{j}}_s = \frac{1}{2}(\hat{v}_x\boldsymbol{\sigma} + \boldsymbol{\sigma}\hat{v}_x). \tag{21}$$

The x-component of the particle current operator reads

$$\hat{j}_p = \hat{v}_x. \tag{22}$$

The current densities can be obtained as expectation values of relevant hermitian operators. The averaging can be performed using the density matrix approach, which is a more suitable method for systems in which the interference effects between the electron states are suppressed. Using independent spin channels approximation, we adopt, in fact, this assumption for the FM material. On the other hand, the well-known fact is that at high temperatures, heavy-fermion compounds exhibit a large saturated resistivity induced by incoherent scattering of the conduction electrons on local magnetic moments. In addition, coherent heavy-electron propagation is readily destroyed by substitutional impurities and thermal fluctuations of the local spins.

The scattering takes place in two independent channels, defined by two spin states of the initial incident electrons. We note that the approach based on the concept of two *noninteracting* spin channels is commonly accepted in the studies of quantum transport in various systems. For spin-independent processes, this spin *degeneracy* leads to a multiplication of final results, such as transmission, conductance, current, etc., by factor 2. However, when the process is spin-dependent, the simple rescaling of results is not justified. In such cases, every spin channel gives, in general, a different contribution to the final result. As a consequence, instead of multiplication by 2, the summation over two spin *degrees of freedom* must be performed. To this end, it is more convenient to use the density matrix formalism, in which this *incoherent* summation over spin channels may be *naturally* included. Moreover, the assumption on the presence of decoherence mechanisms discussed above may also be taken into account easily by neglecting off-diagonal elements in the relevant density matrix. It should be noted here that the calculational procedure described below is fully equivalent to the direct calculation of currents, separately for both channels, from the definition

$$j_x = \tfrac{1}{2}\Big[\psi^\dagger(\hat{v}_x\psi) + (\hat{v}_x\psi)^\dagger\psi\Big], \tag{23}$$

which reduces to the well-known expression for problems without spin–orbit coupling ($\hat{v}_x = p_x/M$)

$$j_x = \tfrac{\mathrm{i}}{2M}\Big[(\nabla_x\psi)^\dagger\psi - \psi^\dagger(\nabla_x\psi)\Big]. \tag{24}$$

However, in order to make all calculations more compact and clear, we use the density matrix approach. In order to construct a spin density matrix for incident electrons, we can introduce the following four-dimensional spin–orbital basis set

$$\Phi_{\mathrm{in}}^{(1)} = \begin{bmatrix} \mathrm{e}^{\,\mathrm{i}\,k_x^{\uparrow}x}\chi^{(\uparrow)} \\ 0 \end{bmatrix}, \quad \Phi_{\mathrm{in}}^{(2)} = \begin{bmatrix} \mathrm{e}^{\,\mathrm{i}\,k_x^{\downarrow}x}\chi^{(\downarrow)} \\ 0 \end{bmatrix},$$
$$\Phi_{\mathrm{in}}^{(3)} = \begin{bmatrix} 0 \\ \mathrm{e}^{\,\mathrm{i}\,k_x^{\uparrow}x}\chi^{(\uparrow)} \end{bmatrix}, \quad \Phi_{\mathrm{in}}^{(4)} = \begin{bmatrix} 0 \\ \mathrm{e}^{\,\mathrm{i}\,k_x^{\downarrow}x}\chi^{(\downarrow)} \end{bmatrix}, \tag{25}$$

where two upper components correspond to the *up* channel, and two lower components correspond to the *down* channel. As a consequence, relevant matrices describing the scattering process have four-dimensional representations. We introduce this construction in order to consider two separate cases, given *together* by (16) and (17). We note that in the channel *up*, only the spin state $\chi^{(\uparrow)}$ appears, and similarly, in the channel *down*, the spin state $\chi^{(\downarrow)}$. The states $\Phi_{\mathrm{in}}^{(2)}$, $\Phi_{\mathrm{in}}^{(3)}$ are required, however, to make the basis set complete. As a consequence, the general state of the incident electron in the four-dimensional *channel-spin* representation (25) reads

$$\Psi_{\mathrm{in}}(y,x) = \mathrm{e}^{\,\mathrm{i}\,k_y y}\Big(\mathrm{e}^{\,\mathrm{i}\,\alpha_1}\,\Phi_{\mathrm{in}}^{(1)} + \mathrm{e}^{\,\mathrm{i}\,\alpha_4}\,\Phi_{\mathrm{in}}^{(4)}\Big), \tag{26}$$

where α_1, α_4 are arbitrary phases. Assuming the existence of some randomization mechanism for phases α_1 and α_4, making the superposition in (26) incoherent, and in consequence, giving two independent scattering channels, the state (26) in the basis (25) may be described by the diagonal density matrix

$$[\hat{\rho}_{\mathrm{in}}] = \begin{bmatrix} \rho_{\mathrm{in}}^{\uparrow} & 0 \\ 0 & \rho_{\mathrm{in}}^{\downarrow} \end{bmatrix},$$
$$\rho_{\mathrm{in}}^{\uparrow} = \begin{bmatrix} 1 & 0 \\ 0 & 0 \end{bmatrix}, \quad \rho_{\mathrm{in}}^{\downarrow} = \begin{bmatrix} 0 & 0 \\ 0 & 1 \end{bmatrix}. \tag{27}$$

One can easily find that the velocity operator $\hat{v}_x$ in the basis (25) has the matrix representation

$$[\hat{v}_{\mathrm{in}}] = \begin{bmatrix} \hat{v}_{\mathrm{in}} & 0 \\ 0 & \hat{v}_{\mathrm{in}} \end{bmatrix}, \quad \hat{v}_{\mathrm{in}} = \begin{bmatrix} \hat{v}_1^{\mathrm{in}} & 0 \\ 0 & \hat{v}_2^{\mathrm{in}} \end{bmatrix}, \tag{28}$$

where

$$\hat{v}_1^{\mathrm{in}} = \frac{k_x^{\uparrow}}{M_1}, \quad \hat{v}_2^{\mathrm{in}} = \frac{k_x^{\downarrow}}{M_1}. \tag{29}$$

In a similar way, for the transmitted electrons, the wave function can be represented as a linear combination of the following four-component functions,

$$\Phi_{\mathrm{tra}}^{(1)} = \begin{bmatrix} \mathrm{e}^{\,\mathrm{i}\,k_{1x}x}\xi^{(1)} \\ 0 \end{bmatrix}, \quad \Phi_{\mathrm{tra}}^{(2)} = \begin{bmatrix} \mathrm{e}^{\,\mathrm{i}\,k_{2x}x}\xi^{(2)} \\ 0 \end{bmatrix},$$
$$\Phi_{\mathrm{tra}}^{(3)} = \begin{bmatrix} 0 \\ \mathrm{e}^{\,\mathrm{i}\,k_{1x}x}\xi^{(1)} \end{bmatrix}, \quad \Phi_{\mathrm{tra}}^{(4)} = \begin{bmatrix} 0 \\ \mathrm{e}^{\,\mathrm{i}\,k_{2x}x}\xi^{(2)} \end{bmatrix}. \tag{30}$$

The wave function of the transmitted electrons has the general form

$$\Psi_{\mathrm{tra}}(y,x) = \mathrm{e}^{\,\mathrm{i}\,k_y y}\Big[\mathrm{e}^{\,\mathrm{i}\,\beta_1}\Big(t_1^{\uparrow}\Phi_{\mathrm{tra}}^{(1)} + t_2^{\uparrow}\Phi_{\mathrm{tra}}^{(2)}\Big) + \mathrm{e}^{\,\mathrm{i}\,\beta_4}\Big(t_1^{\downarrow}\Phi_{\mathrm{tra}}^{(3)} + t_2^{\downarrow}\Phi_{\mathrm{tra}}^{(4)}\Big)\Big], \tag{31}$$

where random phases β_1 and β_4 have again been introduced formally to decouple both channels. We note that for transmitted electrons, intra-channel coherent superpositions of different Rashba states lead to off-diagonal matrix elements in corresponding diagonal blocks of the density

matrix. The off-diagonal terms include the factor $\exp(\mathrm{i}(k_{1x}-k_{2x}^{*})x)$ that leads to x-dependent weekly oscillating terms in the transmitted currents for propagating modes (both k_{1x}, k_{2x} — real). On the other hand, the evanescent modes (one or two of k_{1x}, k_{2x} — complex) do not contribute to the current. Since interference effects are supposed to be rather weak due to the reasons given earlier, we can neglect off-diagonal terms in general, taking in the first approximation of the density operator in the diagonal form. Finally, the corresponding density matrix reads

$$[\hat{\rho}_{\mathrm{tra}}] = \begin{bmatrix} \rho_{\mathrm{tra}}^{\uparrow} & 0 \\ 0 & \rho_{\mathrm{tra}}^{\downarrow} \end{bmatrix},$$

$$\rho_{\mathrm{tra}}^{\uparrow} = \begin{bmatrix} |t_1^{\uparrow}|^2 & 0 \\ 0 & |t_2^{\uparrow}|^2 \end{bmatrix}, \quad \rho_{\mathrm{tra}}^{\downarrow} = \begin{bmatrix} |t_1^{\downarrow}|^2 & 0 \\ 0 & |t_2^{\downarrow}|^2 \end{bmatrix}. \tag{32}$$

The velocity matrix in the basis (30) takes the form

$$[\hat{v}_{\mathrm{tra}}] = \begin{bmatrix} \hat{v}_{\mathrm{tra}} & 0 \\ 0 & \hat{v}_{\mathrm{tra}} \end{bmatrix}, \quad \hat{v}_{\mathrm{tra}} = \begin{bmatrix} \hat{v}_1^{\mathrm{tra}} & 0 \\ 0 & \hat{v}_2^{\mathrm{tra}} \end{bmatrix}, \tag{33}$$

where

$$\hat{v}_1^{\mathrm{tra}} = \frac{\mathrm{Re}(k_{1x})}{M_2} + 2\alpha\frac{\mathrm{Re}(z_1)}{1+|z_1|^2},$$
$$\hat{v}_2^{\mathrm{tra}} = \frac{\mathrm{Re}(k_{2x})}{M_2} - 2\alpha\frac{\mathrm{Re}(z_2)}{1+|z_2|^2}. \tag{34}$$

In the same manner, the density matrix for reflected electrons eigenstates may be constructed. This is not, however, necessary to construct this matrix explicitly because the reflected electrons eigenstates are not independent of transmitted electrons eigenstates, and moreover, we investigate the effects related to the transmission.

We note that from a technical point of view, it is more convenient to consider a finite-width system with periodic boundary conditions instead of an infinite 2D system. Introducing periodic boundary conditions along the y-direction, we obtain discrete values

$$k_y^n = \frac{2\pi}{W}\, n, \quad n = 0, \pm 1, \pm 2, \ldots, \tag{35}$$

where W is the width of the junction. As well known, averaging of any observable is equivalent to calculating the trace of the product of the density operator and relevant observable, taken in the same representation. The (E,n)-resolved spin current and particle current are obtained by taking the following traces,

$$\boldsymbol{j}_s(E,n) = \mathrm{Tr}([\rho][\boldsymbol{j}_s]), \tag{36}$$

$$j_p(E,n) = \mathrm{Tr}([\rho][j_p]), \tag{37}$$

where $[\boldsymbol{j}_s]$ and $[j_p]$ are four-dimensional matrices obtained directly from (21) and (22) using relevant matrix representations for velocity operator and spin operators (see Appendix B). Applying the definitions given above to the incident electrons, we obtain analytical expressions for the spin current

$$\boldsymbol{j}_s^{\mathrm{in}}(E,n) = \frac{k_x^{\uparrow}(E,n) - k_x^{\downarrow}(E,n)}{M_1}\,\boldsymbol{m} \tag{38}$$

and for the particle current

$$j_p^{\mathrm{in}}(E,n) = \frac{k_x^{\uparrow}(E,n) + k_x^{\downarrow}(E,n)}{M_1}. \tag{39}$$

The energy-resolved currents are obtained by summation over discrete transverse modes, numbered by the index n,

$$\boldsymbol{j}_s(E) = \sum_{n=-N}^{N} \boldsymbol{j}_s(E,n), \tag{40}$$

$$j_p(E) = \sum_{n=-N}^{N} j_p(E,n), \tag{41}$$

where $N = \min\left(\mathrm{Int}(\frac{k^{\uparrow\downarrow}W}{2\pi})\right)$. Note that the direction of the vector $\boldsymbol{j}_s$ for the incident electrons is the direction of the magnetization vector $\boldsymbol{m}$. In turn, its magnitude is proportional to the difference of k_x-components of Fermi vectors for the majority and minority carriers. For transmitted electrons, the direction of $\boldsymbol{j}_s$ is, in general, changed relatively to $\boldsymbol{m}$ due to the Rashba spin–orbit interaction. In the presence of interference effects between plane waves corresponding to different Bloch vectors $\boldsymbol{k}_1, \boldsymbol{k}_2$, the spin polarization vector performs continuous precession along the transport direction, like in the Datta–Das spin effect transistor. However, in the present approach, the interference effects are absent for the reasons discussed earlier, and the vector $\boldsymbol{j}_s$ has a constant direction and magnitude that depends only on the initial conditions. From the spintronics point of view, a key question is how large is the spin current normalized to the total particle current. The efficiency of spin polarization is characterized by the ratio of the spin current to the particle current [36], i.e.,

$$P_i(E) = \frac{j_{s,i}(E)}{j_p(E)} \quad (i = x, y, z). \tag{42}$$

For a fixed transverse mode, the spin polarization vector for incident electrons reads

$$\boldsymbol{P}^{\mathrm{in}} = \frac{k_x^{\uparrow} - k_x^{\downarrow}}{k_x^{\uparrow} + k_x^{\downarrow}}\,\boldsymbol{m}. \tag{43}$$

The obtained result is a generalization of the spin polarization of the conductance formula corresponding to a 1D ferromagnet/metal tunnel junction [33]. We see that the magnitude of $\boldsymbol{P}$ is independent of the magnetization direction, and in the absence of the exchange splitting ($k_x^{\uparrow} = k_x^{\downarrow}$), the polarization becomes zero. The summation over transverse modes does not change these properties.

4. Low-bias conductance

To obtain the conductance, we first calculate the transmission coefficient using relevant scattering amplitudes. The transmission coefficient from

the left lead to the right lead is given as $T_{LR} = |j_p^{\rm tra}|/|j_p^{\rm in}|$, where current densities are calculated for a given transverse mode. Taking into account two spin channels separately, we can write

$$T_n^{\uparrow}(E) = \frac{|t_1^{\uparrow}|^2 \hat{v}_1^{\rm tra} + |t_2^{\uparrow}|^2 \hat{v}_2^{\rm tra}}{\hat{v}_1^{\rm in}}, \tag{44}$$

$$T_n^{\downarrow}(E) = \frac{|t_1^{\downarrow}|^2 \hat{v}_1^{\rm tra} + |t_2^{\downarrow}|^2 \hat{v}_2^{\rm tra}}{\hat{v}_2^{\rm in}}, \tag{45}$$

where the index n denotes the transverse mode, parameterized by the value of k_y with periodic boundary conditions. Assuming that the bias voltage V_{LR} is very weak ($T_{LR} \approx T_{RL}$), the electric current I from the left lead to the right lead is given as

$$I = \frac{e}{h} \int\limits_{-\infty}^{\infty} {\rm d}E \sum_n \Big[T_n^{\uparrow}(E) + T_n^{\downarrow}(E)\Big] \times \Big[f(E - E_{\rm F} - eV_{LR}) - f(E - E_{\rm F})\Big], \tag{46}$$

where $f(\cdot)$ is the Fermi distribution function. The summation over transverse modes can be transformed into the integration over the angle $\vartheta = \sin^{-1}(k_y/k_{\rm F})$, according to

$$\sum_n k_y^n \longrightarrow \frac{W}{2\pi} \int\limits_{-k_{\rm F}}^{k_{\rm F}} {\rm d}k_y = \frac{W k_{\rm F}}{2\pi} \int\limits_{-\pi/2}^{\pi/2} {\rm d}\vartheta \cos(\vartheta),$$

$$T_n(E) \longrightarrow T(E, \vartheta), \tag{47}$$

where $k_{\rm F} = k^{\uparrow}$ or $k_{\rm F} = k^{\downarrow}$. Finally, we obtain

$$I = \frac{We}{4\pi^2\hbar} \int\limits_{-\infty}^{\infty} {\rm d}E \int\limits_{-\pi/2}^{\pi/2} {\rm d}\vartheta \, \cos(\vartheta) \times \Big[k^{\uparrow}(E) T^{\uparrow}(E, \vartheta) + k^{\downarrow}(E) T^{\downarrow}(E, \vartheta)\Big] \times \Big[f(E - E_{\rm F} - eV_{LR}) - f(E - E_{\rm F})\Big]. \tag{48}$$

Using the approximation $f(E - E_{\rm F} - eV_{LR}) - f(E - E_{\rm F}) \approx eV_{LR}\,\delta(E - E_{\rm F})$, valid in the zero-bias limit and in the low-temperature limit, we obtain the conductance per unit width of the junction $G = W^{-1}{\rm d}I/{\rm d}V_{LR}$. The total conductance G can be expressed as the sum of two spin-resolved components, corresponding to two spin-channels of incident electrons,

$$G = G^{(\uparrow)} + G^{(\downarrow)}, \tag{49}$$

where

$$G^{(\uparrow)} = \frac{e^2}{2\pi\, h} \int\limits_{-\pi/2}^{\pi/2} {\rm d}\vartheta \, \cos(\vartheta) k^{\uparrow}(E_{\rm F}) T^{\uparrow}(E_{\rm F}, \vartheta),$$

$$G^{(\downarrow)} = \frac{e^2}{2\pi\, h} \int\limits_{-\pi/2}^{\pi/2} {\rm d}\vartheta \, \cos(\vartheta) k^{\downarrow}(E_{\rm F}) T^{\downarrow}(E_{\rm F}, \vartheta), \tag{50}$$

where $E_{\rm F}$ is the equilibrium Fermi level of the junction.

5. Results and discussion

We theoretically studied transport-related issues in terms of the spin current and the charge current through the two-dimensional tunnel junction, composed of ferromagnetic metal and heavy fermion Rashba metal, separated by the thin insulating barrier. The problem has been investigated in a framework of effective mass approximation in combination with density matrix formalism. The spin states have been investigated as devoid of phase coherence due to several mechanisms of decoherence discussed in previous sections. We focused on the analysis of the measure of the spin polarization of the spin current, the particle current dependence, as well as the low-bias conductance dependence on the system characteristic parameters. The measure of the spin

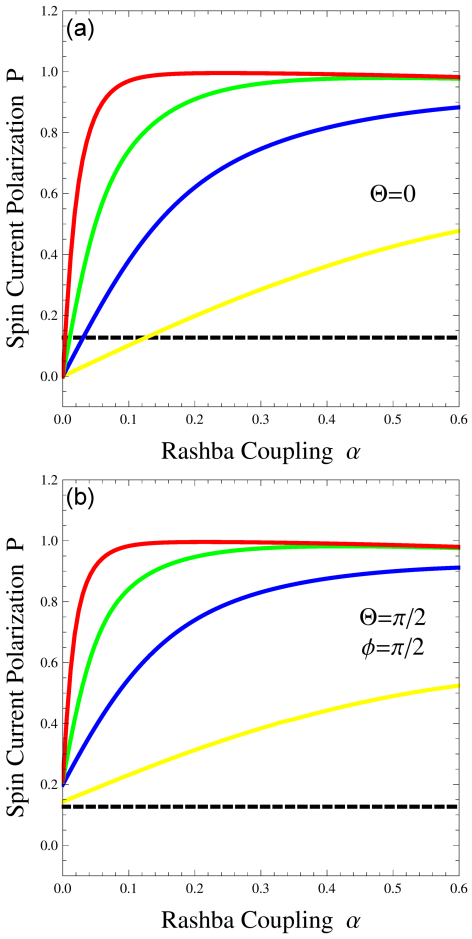

Fig. 3. The magnitude P of the spin current polarization vector (see (42)) for transmitted electrons (solid lines) and incident electrons (black dashed line), for several effective masses M_2 and magnetization directions of FM, given by angles Θ and ϕ. Polarization P is given as a function of Rashba coupling constant α (in units of α_0). The colour curves mean: $M_2 = 1$ (yellow), $M_2 = 10$ (blue), $M_2 = 100$ (green), and $M_2 = 1000$ (red) (in units of m_e). Calculations performed with parameters: $E = 4, E_0 = 0, \Delta = 1, \gamma = 2$ (in atomic units).

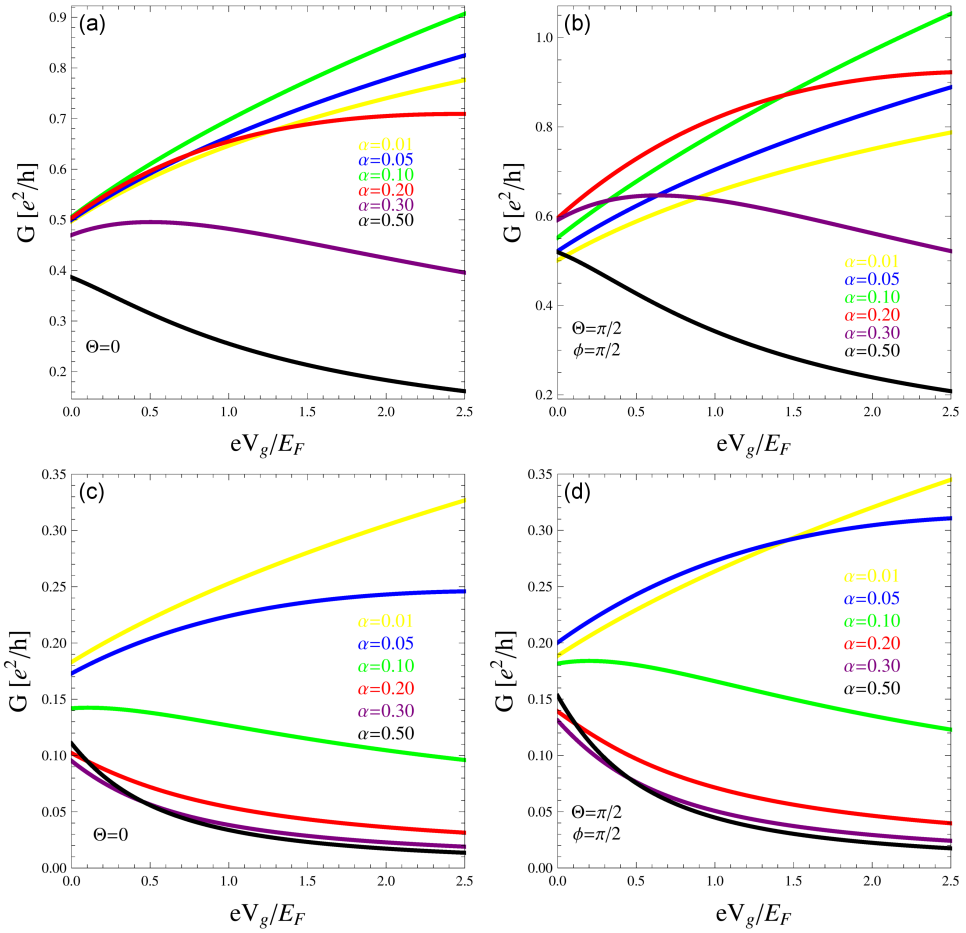

Fig. 4. Conductance G (in units of e^2/h) per unit width of the junction as function of gate voltage V_g: (a), (b) $M_2 = 10$; (c), (d) $M_2 = 100$, for several values of Rashba coupling constant α (in atomic units) with fixed parameters: $E_{\rm F} = 4, \Delta = 1, \gamma = 2$, and orientation of the magnetization vector given by angles (Θ, ϕ).

current polarization is referred to as the efficiency of the spin current polarization, i.e., the quotient of the spin current to the total particle current. According to the definition, this is a vector quantity that is related to the three spin components of the spin current operator. We examined the dependence of the magnitude of this vector on the model parameters for an infinite two-dimensional system with periodic boundary conditions. The total conductance and spin-resolved conductances are studied in the linear response regime.

Figure 3 presents the dependence of the magnitude P of the spin current polarization vector, defined in (42). The dependence of P on Rashba spin–orbit coupling constant α is demonstrated for increasing effective masses of the electron in the HFRM material. Two orientations of the initial spin-polarization vector, defined in (43) are considered: the orientation perpendicular to the plane of the system and the in-plane orientation, which are given in Fig. 3a and Fig. 3b, respectively. We can see that the spin polarization of the current strongly depends on the effective masses difference between the HFRM and FM parts of the junction. In the latter, the effective electron mass is fixed on the value corresponding to the free electron mass ($M_1 = m_e$). For fixed α, the polarization increases with M_2 monotonically. For large M_2, the polarization rapidly increases with α and discloses saturation, approaching the maximal value $P = 1$. We can see that the polarization of the spin current in the case of the in-plane orientation of the magnetization vector ($\Theta = \pi/2, \phi = \pi/2$) exceeds the polarization corresponding to the case of the out-of-plane orientation of the magnetization ($\Theta = 0, \phi$-arbitrary) for every value of α.

Figure 4 presents conductance spectra corresponding to the linear response regime. The spectra are grouped according to the increasing effective mass M_2, different orientations of the magnetization vector in the FM, and several α-values in the HFRM. The spectra are plotted as a function of the ratio $E_0/E_{\rm F}$. In an experimental realization, energy shift $E_0 = eV_g$ is obtained by applying the gate voltage V_g. We can see that the conductance is higher when the magnetization vector of the FM lead lies in the plane of the junction, i.e., when it is parallel to the Rashba magnetic field in the

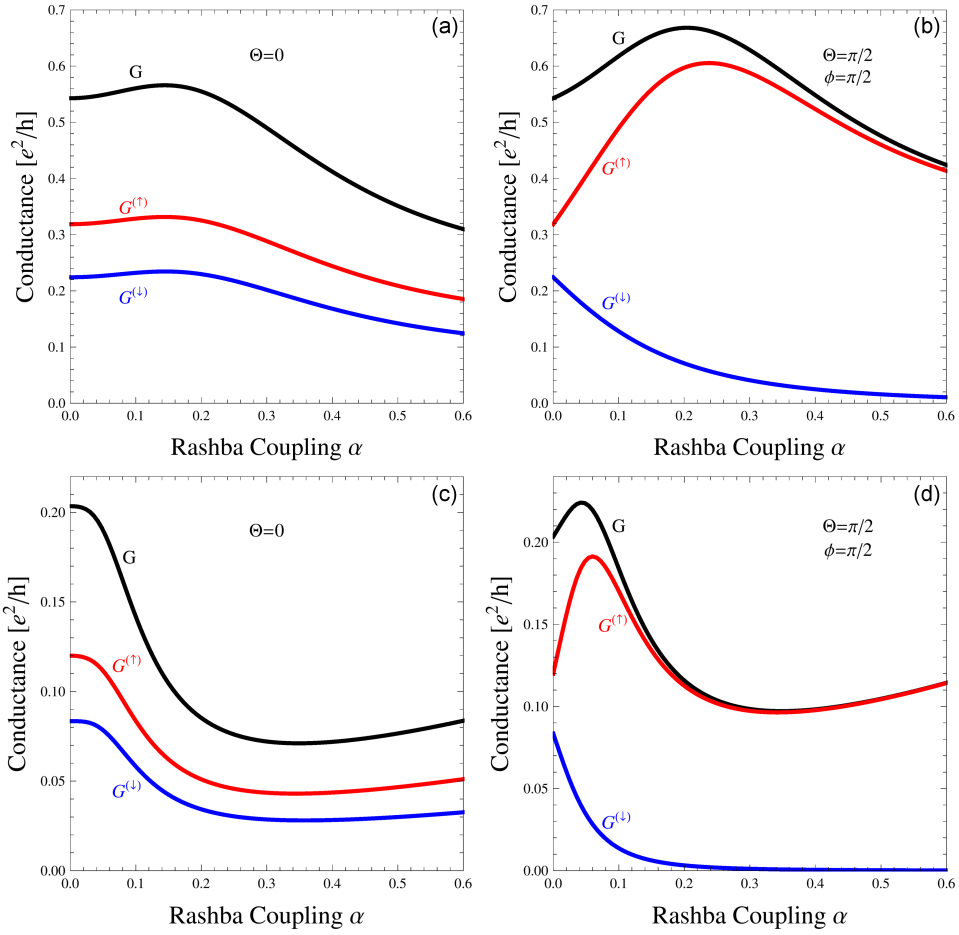

Fig. 5. The total conductance G and spin-resolved conductances $G^{(\uparrow)}$ and $G^{(\downarrow)}$ per unit width of the junction as functions of Rashba coupling α (in atomic units): (a), (b) $M_2 = 10$; (c),(d) $M_2 = 100$. The model parameters: $E_{\mathrm{F}} = 4, \Delta = 1, \gamma = 2$.

HFRM lead. In general, numerical simulations performed for various orientations of the magnetization indicate that the parallel alignment of the polarization vector is the optimal configuration for the highest conductance. For the effective mass $M_2 = 10$, the conductance increases with V_g for a wide range of α. However, for $M_2 = 100$, the conductance decreases with growing V_g when $\alpha \gtrsim 0.1$. In general, the conductance becomes lower as M_2 increases. As a consequence, the electric current is suppressed by the high difference in effective masses between FM and HFRM leads. However, as we have seen, the spin current normalized to the particle current becomes enhanced in this limit. One should note here that the conductance (resistance) is correlated strongly with Rashba spin–orbit coupling, modulated by the external electric field. By switching between low (high) α, we can obtain low (high) resistance of the system. Moreover, the conductance (resistance) difference between states with low and high α may be tuned up by the gate voltage V_g.

Figure 5 presents the α-dependence of total conductance G and spin-resolved conductances $G^{(\uparrow)}$ and $G^{(\downarrow)}$ in the linear response limit. We can see that the dependence of the conductance on Rashba spin–orbit coupling α is strongly correlated with the orientation of the magnetization vector of the FM material. In the case of out-of-plane orientation perpendicular to the plane of the junction, the difference between $G^{(\uparrow)}$ and $G^{(\downarrow)}$ is approximately constant. As we can see in Fig. 5a and c, both components give slightly different contributions to the total conductance. However, in the case of the in-plane orientation of the magnetization vector ($\Theta = \pi/2, \phi = \pi/4$), the component $G^{(\downarrow)}$ decreases to zero with growing α, while the component $G^{(\uparrow)}$ increases. Finally, for sufficiently high Rashba coupling, the total conductance contains only one spin component. Thus, the junction acts as a spin valve, transmitting only one component of the spin-polarized current. The effect is larger for larger mass differences between both parts of the junction. As we can see in panels (b) and (d) in Fig. 5, the $G^{(\downarrow)}$ component is completely filtered out for $\alpha \gtrsim 0.6$ and $\alpha \gtrsim 0.3$ for $M_2 = 10$ and $M_2 = 100$, respectively. By changing the α sign, the components $G^{(\uparrow)}$ and $G^{(\downarrow)}$ exchange their roles.

6. Conclusions

In summary, we have investigated some new aspects related to spin current and charge current in the two-dimensional tunnel device containing ferromagnetic metal as the source electrode and heavy fermion material with Rashba spin–orbit interaction as the drain electrode. We have observed a few peculiar features, important from the point of view of spintronics applications, emerging in the behavior of the spin current polarization and the low-bias conductance. The spin current polarization amplification and spin-resolved conductance have been studied for several sets of macroscopic parameters of the system. In particular, effective filtering of spin currents with opposite spin polarizations was observed as a result of the Rashba spin–orbit coupling occurring in the drain electrode for the system with the in-plane orientation of magnetization in the source electrode.

Appendix A: Scattering coefficients

The scattering amplitudes corresponding to transmitted and reflected electrons satisfy the system of linear equations

$$\begin{bmatrix} c & -s^* & -1 & -1 \\ s & c^* & \mathrm{i}z_1 & -\mathrm{i}z_2 \\ -\frac{\mathrm{i}k_x^{\uparrow}}{M_1}c & \frac{\mathrm{i}k_x^{\downarrow}}{M_1}s^* & \left[\frac{\mathrm{i}k_{1x}}{M_2}(2\alpha M_2 z_1 - 1) + 2\gamma\right] & \left[-\frac{\mathrm{i}k_{2x}}{M_2}(2\alpha M_2 z_2 + 1) + 2\gamma\right] \\ -\frac{\mathrm{i}k_x^{\uparrow}}{M_1}s & -\frac{\mathrm{i}k_x^{\downarrow}}{M_1}c^* & -\left[\frac{k_{1x}}{M_2}(z_1 - 2\alpha M_2) + 2\mathrm{i}\gamma z_1\right] & \left[\frac{k_{2x}}{M_2}(z_2 + 2\alpha M_2) + 2\mathrm{i}\gamma z_2\right] \end{bmatrix} \begin{bmatrix} r_p^{\uparrow} \\ r_a^{\uparrow} \\ \tilde{t}_1^{\uparrow} \\ \tilde{t}_2^{\uparrow} \end{bmatrix} = \begin{bmatrix} -c \\ -s \\ -\frac{\mathrm{i}k_x^{\uparrow}}{M_1}c \\ -\frac{\mathrm{i}k_x^{\uparrow}}{M_1}s \end{bmatrix} \tag{51}$$

for the channel (↑) and

$$\begin{bmatrix} -s^* & c & -1 & -1 \\ c^* & s & \mathrm{i}z_1 & -\mathrm{i}z_2 \\ \frac{\mathrm{i}k_x^{\downarrow}}{M_1}s^* & -\frac{\mathrm{i}k_x^{\uparrow}}{M_1}c & \left[\frac{\mathrm{i}k_{1x}}{M_2}(2\alpha M_2 z_1 - 1) + 2\gamma\right] & \left[-\frac{\mathrm{i}k_{2x}}{M_2}(2\alpha M_2 z_2 + 1) + 2\gamma\right] \\ -\frac{\mathrm{i}k_x^{\downarrow}}{M_1}c^* & -\frac{\mathrm{i}k_x^{\uparrow}}{M_1}s & -\left[\frac{k_{1x}}{M_2}(z_1 - 2\alpha M_2) + 2\mathrm{i}\gamma z_1\right] & \left[\frac{k_{2x}}{M_2}(z_2 + 2\alpha M_2) + 2\mathrm{i}\gamma z_2\right] \end{bmatrix} \begin{bmatrix} r_p^{\downarrow} \\ r_a^{\downarrow} \\ \tilde{t}_1^{\downarrow} \\ \tilde{t}_2^{\downarrow} \end{bmatrix} = \begin{bmatrix} s^* \\ -c^* \\ \frac{\mathrm{i}k_x^{\downarrow}}{M_1}s^* \\ -\frac{\mathrm{i}k_x^{\downarrow}}{M_1}c^* \end{bmatrix} \tag{52}$$

for the channel (↓). The transmission coefficients $t_i^{\uparrow\downarrow} = \tilde{t}_i^{\uparrow\downarrow}\sqrt{1+|z_i|^2}$ for $i = 1, 2$.

Appendix B: Spin matrices in channel-spin representation

The spin matrices corresponding to incident electrons in the representation (25) read

$$[\sigma_1^{\mathrm{in}}] = \begin{bmatrix} \sigma_1^{\mathrm{in}} & 0 \\ 0 & \sigma_1^{\mathrm{in}} \end{bmatrix}, \quad [\sigma_2^{\mathrm{in}}] = \begin{bmatrix} \sigma_2^{\mathrm{in}} & 0 \\ 0 & \sigma_2^{\mathrm{in}} \end{bmatrix}, \quad [\sigma_3^{\mathrm{in}}] = \begin{bmatrix} \sigma_3^{\mathrm{in}} & 0 \\ 0 & \sigma_3^{\mathrm{in}} \end{bmatrix}, \tag{53}$$

where

$$\sigma_1^{\mathrm{in}} = \begin{bmatrix} \sin(\vartheta)\cos(\varphi) & 0 \\ 0 & -\sin(\vartheta)\cos(\varphi) \end{bmatrix}, \quad \sigma_2^{\mathrm{in}} = \begin{bmatrix} \sin(\vartheta)\sin(\varphi) & 0 \\ 0 & -\sin(\vartheta)\sin(\varphi) \end{bmatrix}, \quad \sigma_3^{\mathrm{in}} = \begin{bmatrix} \cos(\vartheta) & 0 \\ 0 & -\cos(\vartheta) \end{bmatrix}. \tag{54}$$

For transmitted electrons, the spin matrices in the representation (30) take forms

$$[\sigma_1^{\mathrm{tra}}] = \begin{bmatrix} \sigma_1^{\mathrm{tra}} & 0 \\ 0 & \sigma_1^{\mathrm{tr}} \end{bmatrix}, \quad [\sigma_2^{\mathrm{tra}}] = \begin{bmatrix} \sigma_2^{\mathrm{tra}} & 0 \\ 0 & \sigma_2^{\mathrm{tr}} \end{bmatrix}, \quad [\sigma_3^{\mathrm{tra}}] = \begin{bmatrix} \sigma_3^{\mathrm{tra}} & 0 \\ 0 & \sigma_3^{\mathrm{tr}} \end{bmatrix}, \tag{55}$$

where

$$\sigma_1^{\mathrm{tra}} = \begin{bmatrix} \frac{2}{1+|z_1|^2}\,\mathrm{Im(z_1)} & 0 \\ 0 & -\frac{2}{1+|z_2|^2}\,\mathrm{Im(z_2)} \end{bmatrix}, \quad \sigma_2^{\mathrm{tra}} = \begin{bmatrix} -\frac{2}{1+|z_1|^2}\,\mathrm{Re(z_1)} & 0 \\ 0 & \frac{2}{1+|z_2|^2}\,\mathrm{Re(z_2)} \end{bmatrix}, \quad \sigma_3^{\mathrm{tra}} = \begin{bmatrix} \frac{1-|z_1|^2}{1+|z_1|^2} & 0 \\ 0 & \frac{1-|z_2|^2}{1+|z_2|^2} \end{bmatrix}. \tag{56}$$

References

[1] E.I. Rashba, *Fiz. Tverd. Tela (Leningrad)* **2**, 1224 (1960).

[2] Y.A. Bychkov, E.I. Rasbha, *P. Zh. Eksp. Teor. Fiz.* **39**, 66 (1984).

[3] R. Winkler, *Spin–orbit Coupling Effects in Two-Dimensional Electron and Hole Systems*, Springer, New York 2003.

[4] G. Bihlmayer, O. Rader, R. Winkler, *New J. Phys.* **17**, 050202 (2015).

[5] X. Liu, J.D. Burton, M.Y. Zhuravlev, E.Y. Tsymbal, *Phys. Rev. Lett.* **114**, 046601 (2015).

[6] S. Datta, B. Das, *Appl. Phys. Lett.* **56**, 665 (1990).

[7] P.R. Hammar, B.R. Bennett, M.J. Yang, M. Johnson, *Phys. Rev. Lett.* **83**, 203 (1999).

[8] P. R. Hammar, M. Johnson, *Phys. Rev. B* **61**, 7207 (2000).

[9] C.-M. Hu, J. Nitta, A. Jensen, J.B. Hansen, H. Takayanagi, *Phys. Rev. B* **63**, 125333 (2001).

[10] A.T. Filip, B.H. Hoving, F.J. Jedema, B.J. van Wees, B. Dutta, S. Borghs, *Phys. Rev. B* **62**, 9996 (2000).

[11] I. Žutić, J. Fabian, S. Das Sarma, *Rev. Mod. Phys.* **76**, 323 (2004).

[12] D. Awschalom, M. Flatté, *Nat. Phys.* **3**, 153159 (2007).

[13] E.Y. Tsymbal, O.N. Mryasov, P.R. LeClair, *J. Phys. Condensed Matter* **15**, R109 (2003).

[14] A. Alexandrov, M.Y. Zhuravlev, E.Y. Tsymbal, *Phys. Rev. Appl.* **12**, 024056 (2019).

[15] M.Y. Zhuravlev, S. Maekawa, E.Y. Tsymbal, *Phys. Rev. B* **81**, 104419 (2010).

[16] A. Jantayod, P. Pairor, *Physica E* **48**, 111 (2013).

[17] S.M. Faraza, Z. Tajwara, Q. ul Wahabb, A. Ulyashinc, R. Yakimovab, *Acta Phys. Pol. A* **141**, 99 (2022).

[18] P. Wiśniewski, B. Majkusiak, *Acta Phys. Pol. A* **140**, 186 (2021).

[19] Z.C. Dong, D.Y. Xing, J. Dong, *Phys. Rev. B* **65**, 214512 (2002).

[20] Z.C. Dong, R. Shen, Z.M. Zheng, D.Y. Xing, Z.D. Wang, *Phys. Rev. B* **67**, 134515 (2003).

[21] L. Gen-Hua, Z. Guang-Hui, *Chinese Phys. Lett.* **22**, 3159 (2005).

[22] M. Lee, M.-S. Choi, *Phys. Rev. B* **71**, 153306 (2005).

[23] V.M. Ramaglia, D. Bercioux, V. Cataudella, G. De Filippis, C.A. Perroni, F. Ventriglia, *Eur. Phys. J. B* **36**, 365375 (2003).

[24] C.M. Hu, T. Matsuyama, *Phys. Rev. Lett.* **87**, 066803 (2001).

[25] T. Matsuyama, C.-M. Hu, D. Grundler, G. Meier, U. Merkt, *Phys. Rev. B* **65**, 155322 (2002).

[26] Y. Jiang, M.B.A. Jalil, *J. Phys. Condensed Matter* **15**, L31 (2003).

[27] D. Oshima, K. Taguchi, Y. Tanaka, *J. Phys. Soc. Jpn.* **87**, 034710 (2018).

[28] T. Yokoyama, Y. Tanaka, J. Inoue, *Phys. Rev. B* **74**, 035318 (2006).

[29] V. Shaginyan, M. Amusia, A. Msezane, K. Popov, *Phys. Rep.* **492**, 31 (2010).

[30] H. Kronmuller, S. Parkin, *Handbook of Magnetism and Advanced Magnetic Materials; Vol. 1: Fundamentals and Theory*, John Wiley and Sons, 2007.

[31] P. Coleman arXiv:1509.05769 (2015).

[32] P. Gegenwart, Q. Si, F. Steglich, *Nat. Phys* **4**, 186197 (2008).

[33] A. Poszwa, *Phys. Scr.* **93**, 025102 (2018).

[34] K. Pasanai, P. Pairor, *Phys. Rev. B* **84**, 224432 (2011).

[35] J. Shi, P. Zhang, D. Xiao, Q. Niu, *Phys. Rev. Lett.* **96**, 076604 (2006).

[36] B. Srisongmuang, P. Pairor, M. Berciu, *Phys. Rev. B* **78**, 155317 (2008).